Vertical and Horizontal Stability of a Bouncing Ball on an Oscillating Surface

by
Eric Bell

ME 399
7 June, 2010

I. Introduction.

The behavior of a bouncing ball on an oscillating surface is a very basic problem in nonlinear dynamics that been studied in great depth. In particular, this problem has generated interest due to the existence of stable fixed points which may lead to bifurcations at certain forcing frequencies and amplitudes. For example, a ball bouncing on the surface of a one degree of freedom oscillating bar with sinusoidal motion in the vertical direction may fall into a pattern in which impacts occur at the same frequency as the bar's motion. The ball will bounce to the same height every time. This pattern is known as a period one motion. If one were to increase the forcing amplitude, the ball would continue in this fashion due to the existence of a stable fixed point. For certain amplitude, however, this fixed point will bifurcate, creating two fixed points. The existence of two stable fixed points will cause a period two to emerge, with the ball alternating between two different heights.

The majority of research on the bouncing ball, however, has focused purely on vertical stability, with little thought given to the side-to-side motion of the ball. The focus of this independent study was to investigate the dynamics of the bouncing ball problem with respect to stability in both the vertical and horizontal directions. By adding periodic motion in the angular and horizontal directions, it was possible to analyze stability in the horizontal direction as well as the vertical. These investigations were conducted using both Matlab simulations and an experimental setup consisting of a three degree of freedom oscillating bar. The ultimate goal of the project was to be able to use the knowledge of stability to control the side-to-side motion of the ball as it is bouncing.

II. Experimental Setup.

In order to observe the behavior of the bouncing ball, a setup was used similar to the system employed in the paper *Chaotic Dynamics of a Bouncing Ball* by Tufillaro and Albano. Low curvature lenses or troughs were used to stabilize any undesirable motions. Concave lenses with focal lengths of 15 and 20 cm were used in the experiments. As shown in Figure 1, a lens is attached to a horizontal bar controlled by four speakers acting as actuators. The four speakers can be used to create periodic motions in three degrees of freedom: vertical, horizontal, and angular. The motion of the bar is controlled by two accelerometers located on either end of the bar. The major difference between the Tufillaro-Albano apparatus and this setup is the method of data capture. In Tufallaro and Albano's experiment, a piezoelectric crystal is used to measure the force of impact between the ball and the lens. The assumption is made that ball amplitude is proportional to the impact force. In contrast, this setup uses a high speed camera to visually capture the ball and calculate its real world coordinates based on its location in the camera frame. This has the advantage of allowing the experimenter to directly observe the object trajectories. Furthermore, the system can track multiple regions, making it possible to view both the path of the ball and the path of the bar. It also has applications for tracking more complicated polygons as well as imaging in three dimensions.

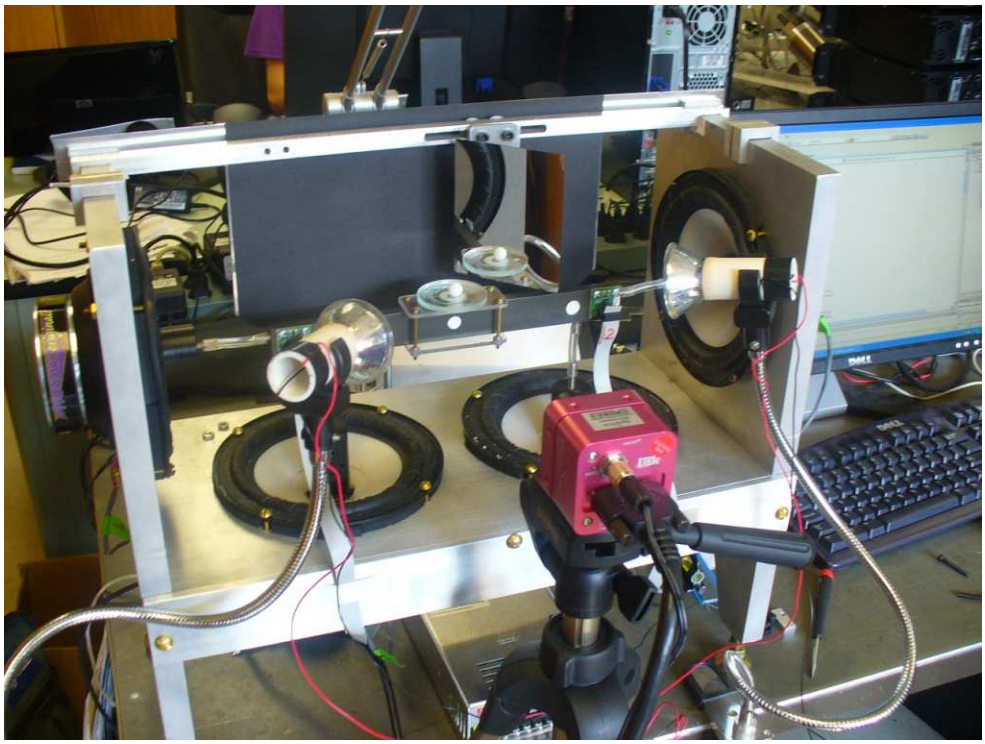

Figure 2.1. Experimental Setup, Arranged for Three Dimensional Imaging

The high speed vision system is capable of capturing data in the kilohertz range. Due to the extremely brief exposure time, powerful lights were necessary in order to capture a usable image. The vision system works by applying a threshold to the grayscale images. As a result, it is able to pick out the white ball against the black background. It then calculates the area centroid

based on the number of white pixels. The bar also has several white fiduciary markers which are used to track the bar's position.

The vision system is most commonly used for tracking the motion of an object in a plane parallel to the image plane of the camera. However, as shown in Figure 2.2, the camera can also be used for 3D imaging by using a small mirror placed at a 45 degree angle to create a second "virtual" camera. By combining data from the two cameras, it is possible to calculate the position of the ball in three dimensions. Figure 2.2 shows an illustration of this concept.

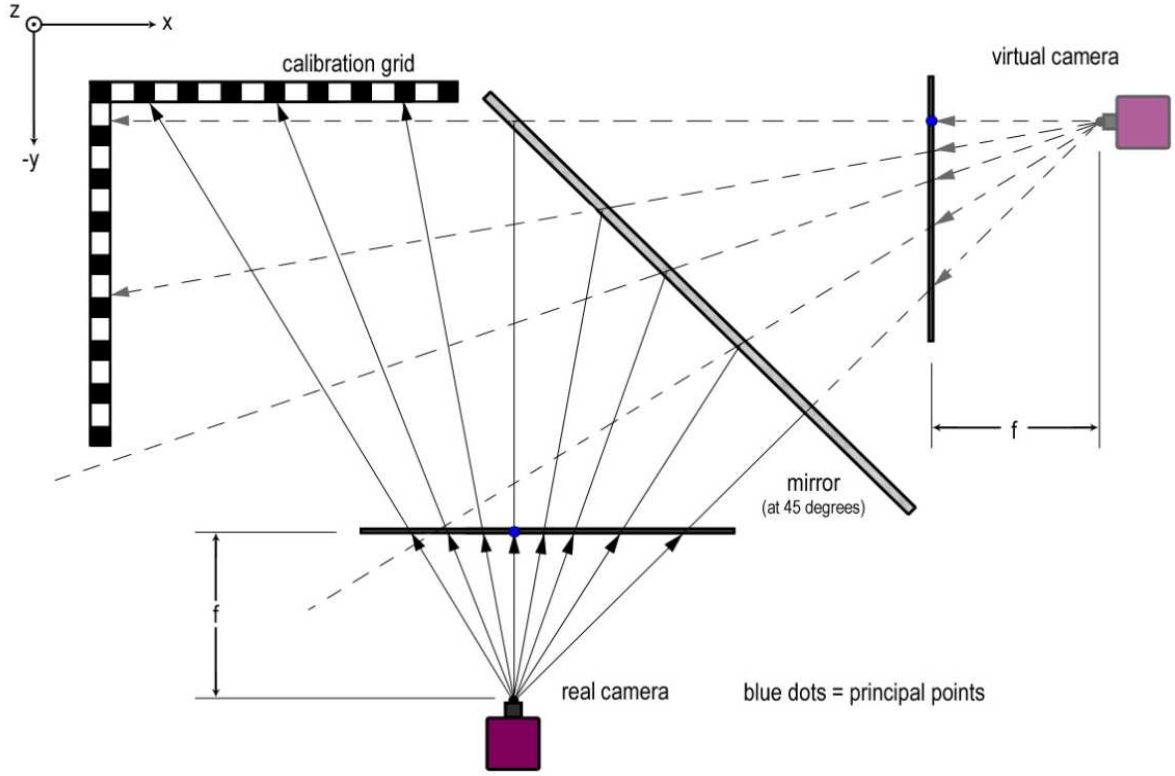

Figure 2.2. Image Tracking in Three Dimensions

As illustrated, the inclusion of the mirror creates two lines of sight which can be used to pinpoint the location of the object of interest by using a least squares calculation. Using a mirror instead of purchasing a second camera provides a cheap alternative for 3D object tracking. The only disadvantage is a slight loss in resolution for the reflected image, which proved inconsequential for these experiments.

The coordinate system shown in Figure 2.2 will be the convention that will be used for the remainder of this report. Positive x will point along the bar from left to right. The y direction will point along the line of sight of the camera, with positive being away from the camera. The positive z axis will be straight up, opposing gravity.

The three dimensional object tracking provides the advantage of being able to observe the horizontal excursions of the ball as well as the height of each bounce. Figures 2.3 and 2.4 demonstrate this concept by showing the three-dimensional position of the ball in time.

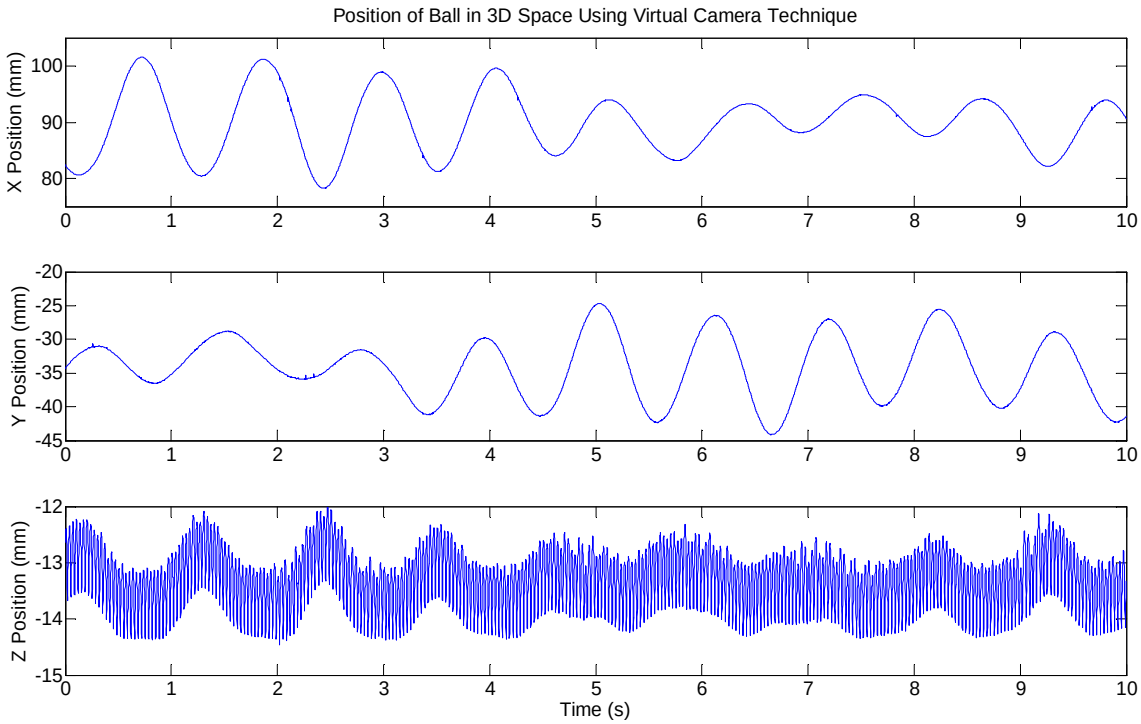

Figure 2.3. X,Y, and Z Positions of the Ball Versus Time.

This data can be used to observe the oscillatory motion of the ball in the XY plane as it is bouncing. Figure 2.4 uses the data from the first two plots in Figure 2.3 to calculate the radial position of the ball in time. As shown in the figure, the ball often travels around the lens at a frequency lower than that of the impact frequency, and the 3D imaging allows us to study these motions.

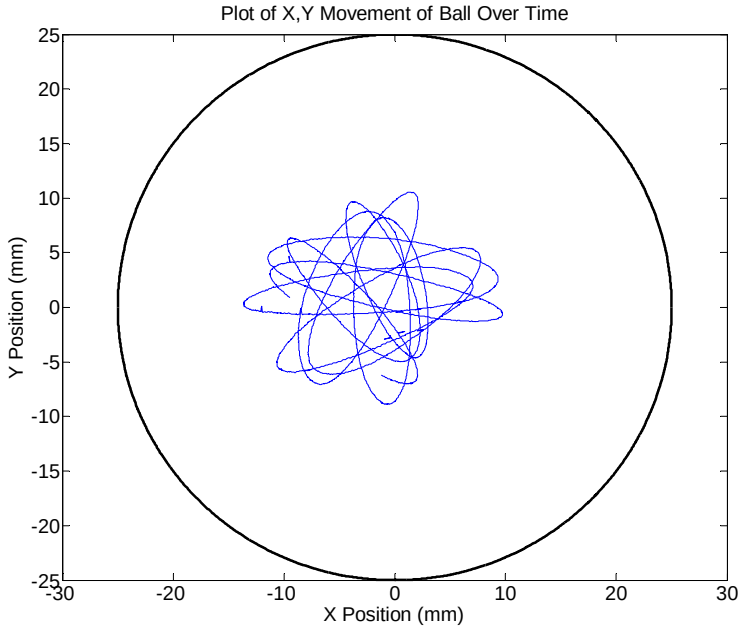

Figure 2.4. Motion of the Ball in the XY Plane

The ability to capture the position of the ball in three dimensions also provides the advantage of being able to adjust the ball's height over time. One disadvantage of using a concave lens is the variable height of the surface. The lens is thinner in the middle, and thicker towards the edge. This causes fluctuations in the z position data as evidenced by the third plot in Figure 2.3. However, since the both position of the ball in the plane of the lens and the lens geometry are known, it is possible to adjust for this variable z offset.

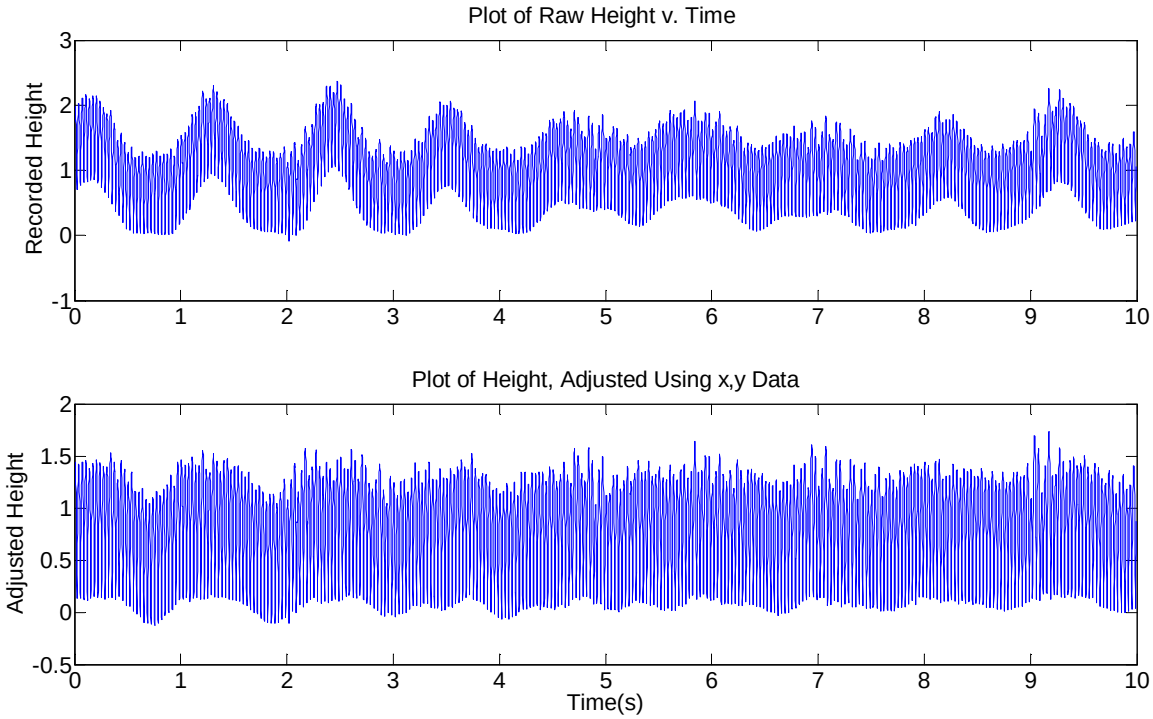

Figure 2.5. Z Position of the Ball v. Time, Before and After Height Adjustment

The first plot in Figure 2.5 shows the original z v. t data with the z position clearly fluctuating as a result of the lens curvature. The second plot was created by adjusting the z offset based on the x and y positions of the bar. Clearly, although not perfect, this method is very effective in reducing the error in ball height and demonstrates the proficiency of the 3D vision system. A complete explanation of how to calibrate and use the vision system can be found on the Mechatronics wiki under Projects and Miscellaneous→ High Speed Vision System and Object Tracking.

III. Vertical Stability.

The first experiments conducted with the high speed vision system attempted to capture examples of stable behaviors such as period 1 and period 2 motions. The investigation began with the simplest possible case; that of the period 1 where the bouncing ball comes into contact with the bar as the same frequency as the bar's oscillation. For the data that follows, the vision system was calibrated for two dimensional imaging. It was running at a frequency of 1000Hz, alternating between two regions of interest. Therefore, data for both the ball the bar were collected at a 500Hz sampling rate. Each parabolic trajectory or cycle of the bar is defined by about 17 data points.

A. Period 1 Motion.

An example of an experimentally obtained period 1 is displayed in Figure 3.1.

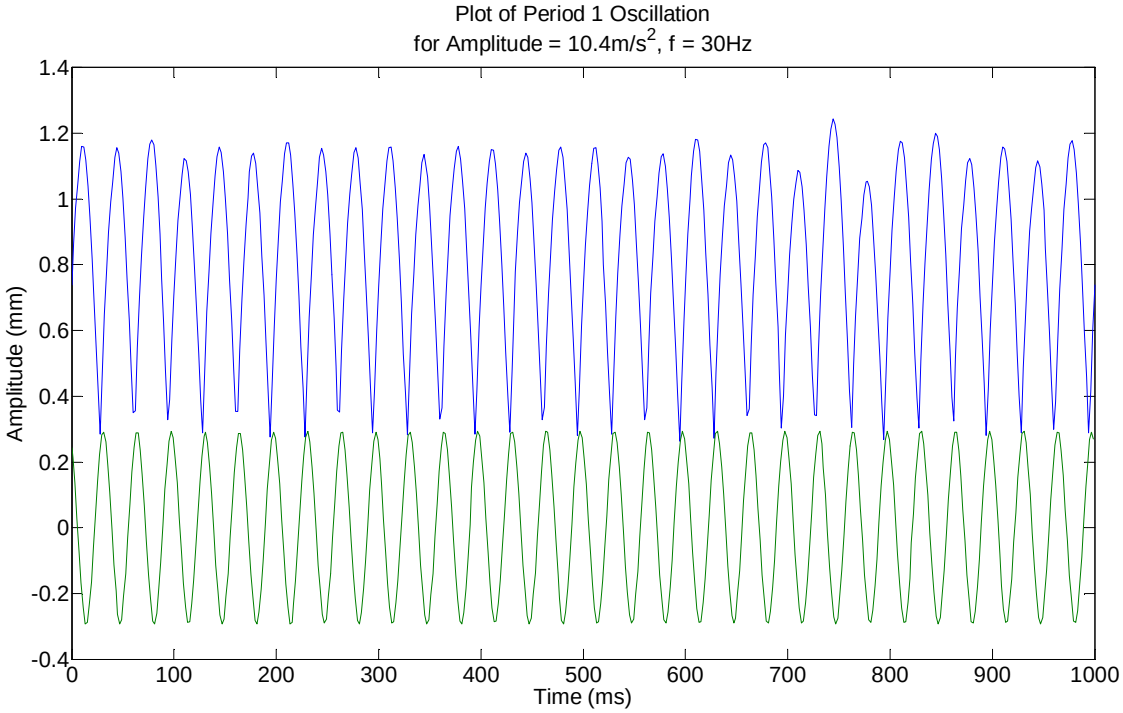

Figure 3.1. Period 1 Behavior as Captured by the Vision System

As shown in the figure, for 1 second of data collection, the ball impacts the bar 30 times for a 30Hz bar frequency. The motion of the bar was defined to be

$$z_{BAR}(t) = A * \sin(\omega t + \varphi)$$

where A is equal to the position amplitude given by the equation

$$A = \frac{Acc}{(2\pi f)^2}$$

Acc is equal to the maximum acceleration of the bar, which in this case was 10.4m/s^2.

In order to obtain more accurate values for the maxima and minima, parabolic fits were calculated for each bounce. The fitted data and resulting maxima and minima are shown in Figure 3.2.

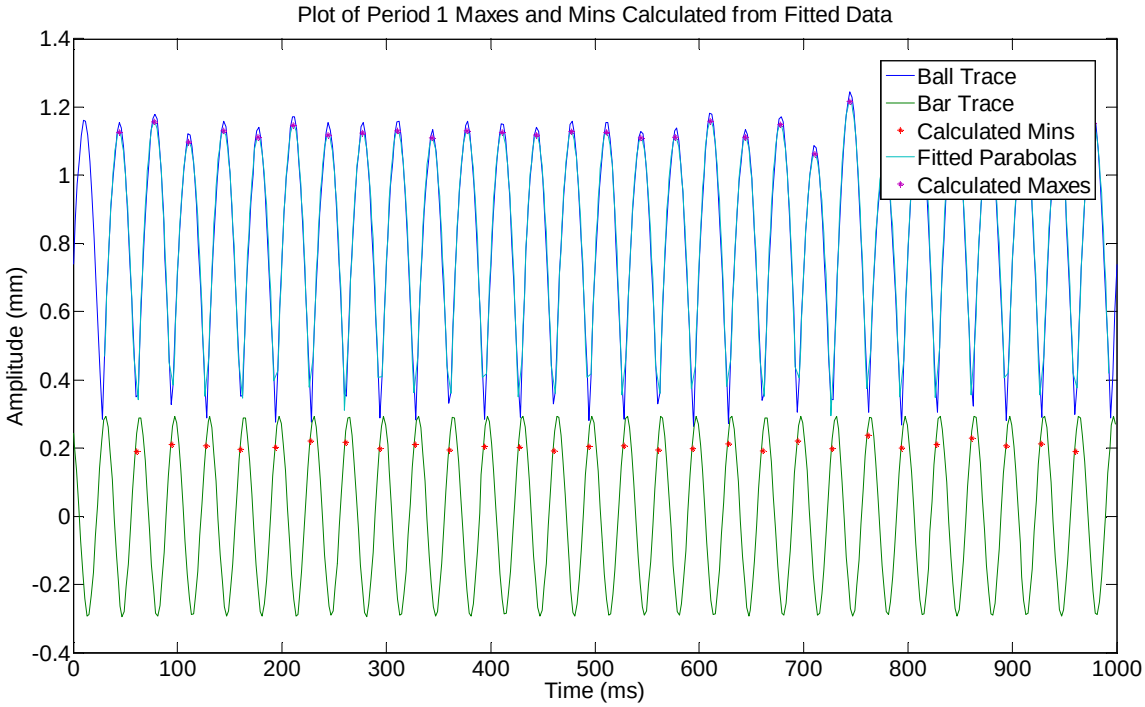

Figure 3.2. Period 1 Fitted Data with Maxima, Minima

The results of the data analysis are shown in Table 3.1. For a period 1 motion at 10.4m/s^2, the ball impacts the bar at an average phase of 0.97 radians. This value seems intuitive since the ball is clearly impacting the bar in the first quarter of the bar's sin wave. Therefore, the ball should impact somewhere in between 0 and pi/2 radians.

IMPACT NUMBER	MAXIMA (mm)	MINIMA (mm)	PHASE AT IMPACT (radians)
1	1.127	0.190	0.941
2	1.157	0.211	1.008
3	1.096	0.206	0.974
4	1.130	0.196	0.939
5	1.112	0.203	0.937
6	1.148	0.220	0.994
7	1.118	0.216	1.008
8	1.124	0.199	0.963
9	1.131	0.211	0.984
10	1.109	0.194	0.925
11	1.131	0.205	0.960
12	1.126	0.203	0.985
13	1.118	0.191	0.926
14	1.128	0.205	0.967
15	1.126	0.206	0.995

16	1.109	0.195	0.933
17	1.111	0.198	0.925
18	1.159	0.213	1.028
19	1.111	0.193	0.960
20	1.149	0.220	1.002
21	1.063	0.198	0.917
22	1.216	0.237	1.097
23	1.043	0.200	0.902
24	1.153	0.211	0.980
25	1.175	0.228	1.092
26	1.099	0.207	0.988
27	1.134	0.212	1.005
28	1.096	0.189	0.927
AVG	1.125	0.206	0.974
STD	0.033	0.012	0.048

Table 3.1: Maxima, Minima, and Impact Phase for Period 1

B. Period 2 Motion.

If one were to increase the amplitude of the bar, the average phase at impact will approach the critical value of pi/2, or 1.57 radians. Once this value is reached, a bifurcation will occur and pattern will change to a period 2, as shown in the figure below.

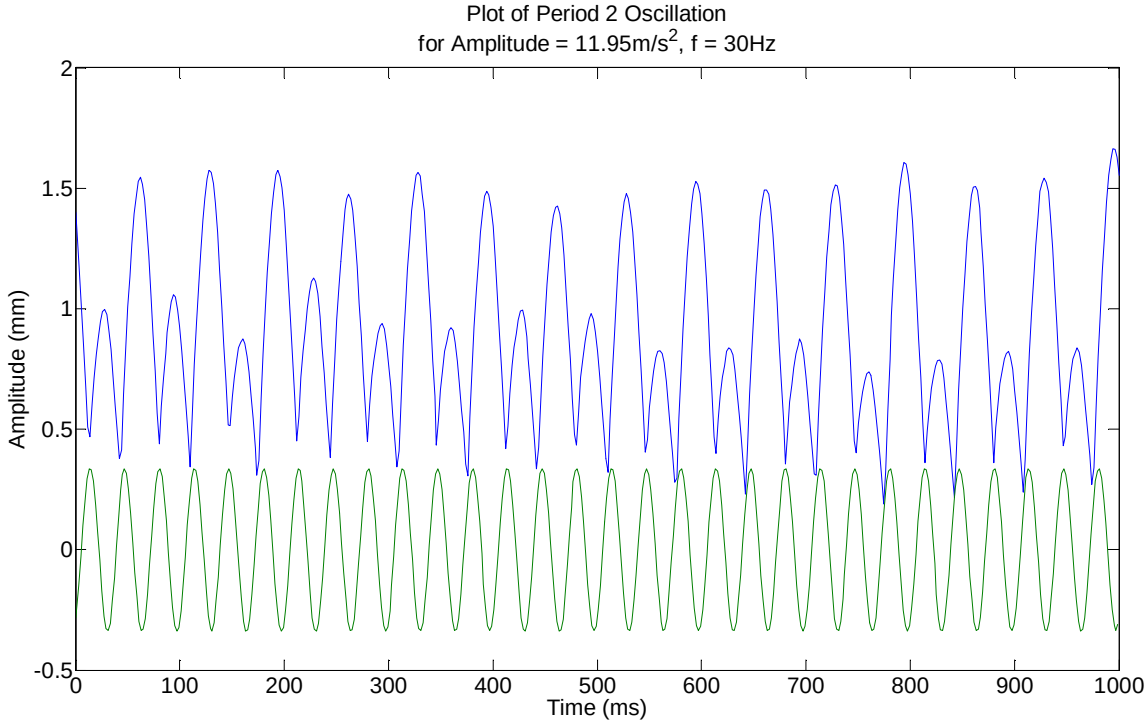

Figure 3.3. Period 2 Behavior as Captured by the Vision System

The period two is characterized by bounces of alternating amplitudes. The ball still impacts the bar once a cycle, however in one second, there are 15 high bounces, and 15 low bounces. The same analysis conducted for the period 1 produced the following:

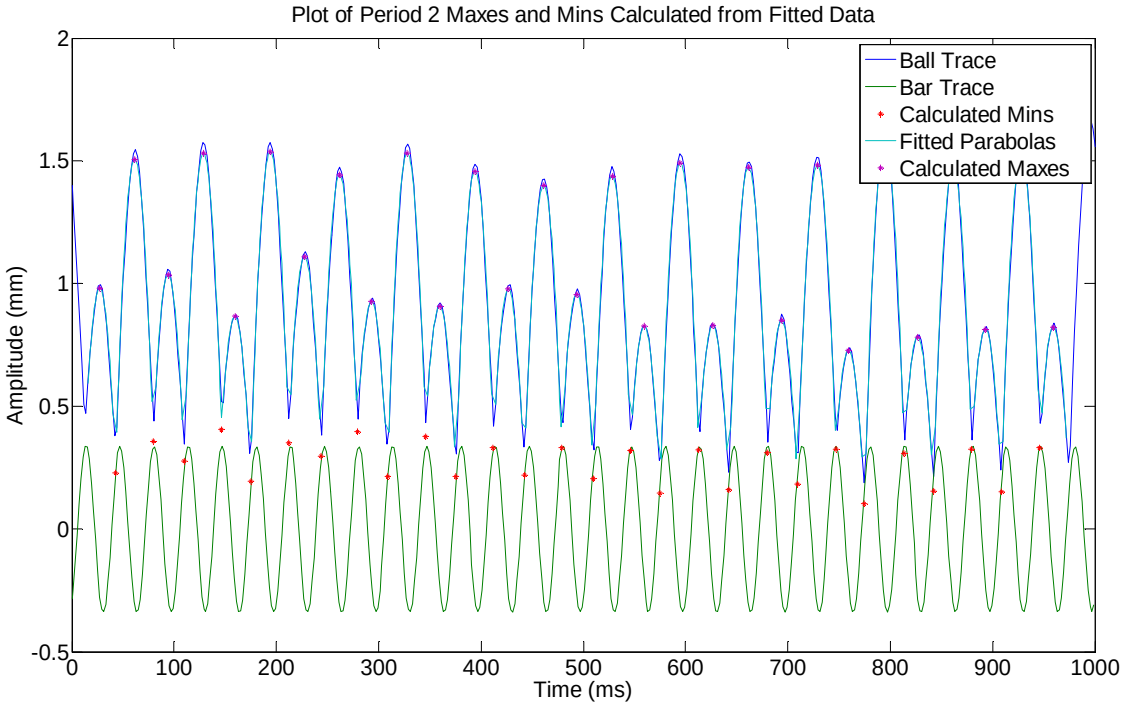

Figure 3.4. Period 2 Fitted Data with Maxima, Minima

IMPACT NUMBER	MAXIMA (mm)	MINIMA (mm)	PHASE AT IMPACT (radians)
1	0.9821	0.2295	0.7394
2	1.5045	0.3563	1.3465
3	1.0336	0.2754	0.8278
4	1.5311	0.4059	1.429
5	0.8656	0.1932	0.5038
6	1.5374	0.3508	1.2007
7	1.1078	0.2979	0.9058
8	1.4422	0.3972	1.3178
9	0.927	0.2149	0.6104
10	1.5318	0.3773	1.3002
11	0.9077	0.2136	0.6377
12	1.4573	0.3296	1.213
13	0.9774	0.2192	0.7028
14	1.399	0.3319	1.2576
15	0.9564	0.2068	0.7874
16	1.4383	0.3198	1.3642
17	0.8266	0.1453	0.5602

18	1.4914	0.3235	1.3943
19	0.8297	0.1609	0.6402
20	1.4728	0.3123	1.409
21	0.8506	0.1823	0.7451
22	1.4824	0.3255	1.505
23	0.7281	0.1029	0.4955
24	1.5719	0.309	1.5054
25	0.7818	0.1529	0.6364
26	1.4816	0.3245	1.3979
27	0.814	0.1512	0.6123
28	1.5148	0.3313	1.3851
AVG(ODDS)	0.9579	0.1961	0.6718
STD(ODDS)	0.1028	0.0524	0.1196
AVG(EVENS)	1.4897	0.3425	1.359
STD(EVENS)	0.0464	0.0309	0.0943

Table 3.2: Maxima, Minima, and Impact Phase for Period 2

As indicated by Table 3.2, for a period 2 at amplitude of 11.95m/s^2, the ball will impact the bar with alternating phases of 0.67 and 1.36. In this case, the smaller value is indicative of a larger bounce and the larger value indicates a smaller bounce. This is because the larger of the two, 1.36 is very close to the bar's zero velocity phase of 1.57, so the bar hits the ball with less energy on these bounces.

C. Beyond Period 2.

Other types of stable periodic motion exist as well, such as a period 3. Period threes are more difficult to predict, but seem to occur when the ball is transitioning from one behavior to another, or at high amplitudes when the ball is in chaos.

Figure 3.5 shows 1 second of a period 3 motion captured by the vision system. This data was taken using 3D imaging with the vision system set to 2000Hz divided over 3 regions of interest. This is the equivalent of a 667Hz sampling rate.

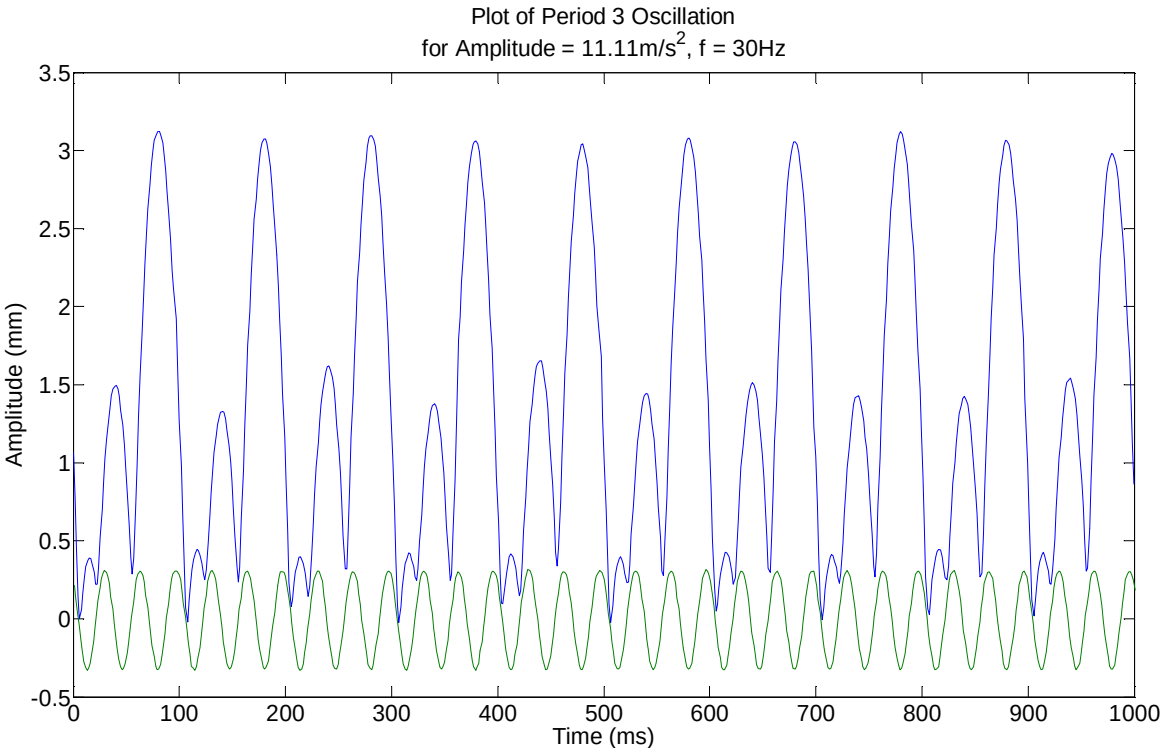

Figure 3.5. Period 3 Behavior as Captured by the Vision System

The same pattern can be observed for higher energy behavior. For example, by changing the initial conditions of the experiment, it is possible to induce a Period 1 type behavior where the ball is coming into contact with the bar exactly once every two cycles of the bar. This is known as a Period 1, m = 2, where m is an integer value representing the ratio of ball bounces to bar cycles. In order to achieve this motion, the ball requires a larger initial energy, and generally higher forcing amplitude. An example of a Period 1, m = 2 captured by the vision system is shown in Figure 3.6.

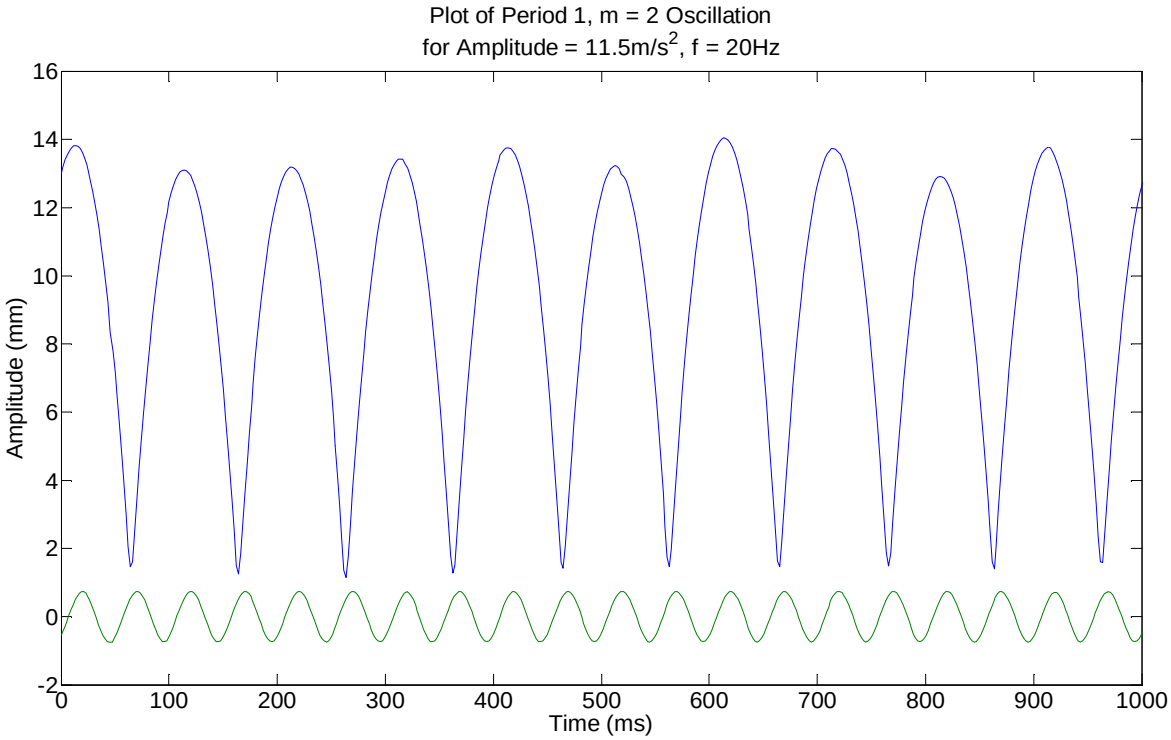

Figure 3.6. Period 1 Behavior with m = 2 as Captured by the Vision System

Furthermore, there exists Period 2 behavior for m = 2 as shown in Figure 3.7.

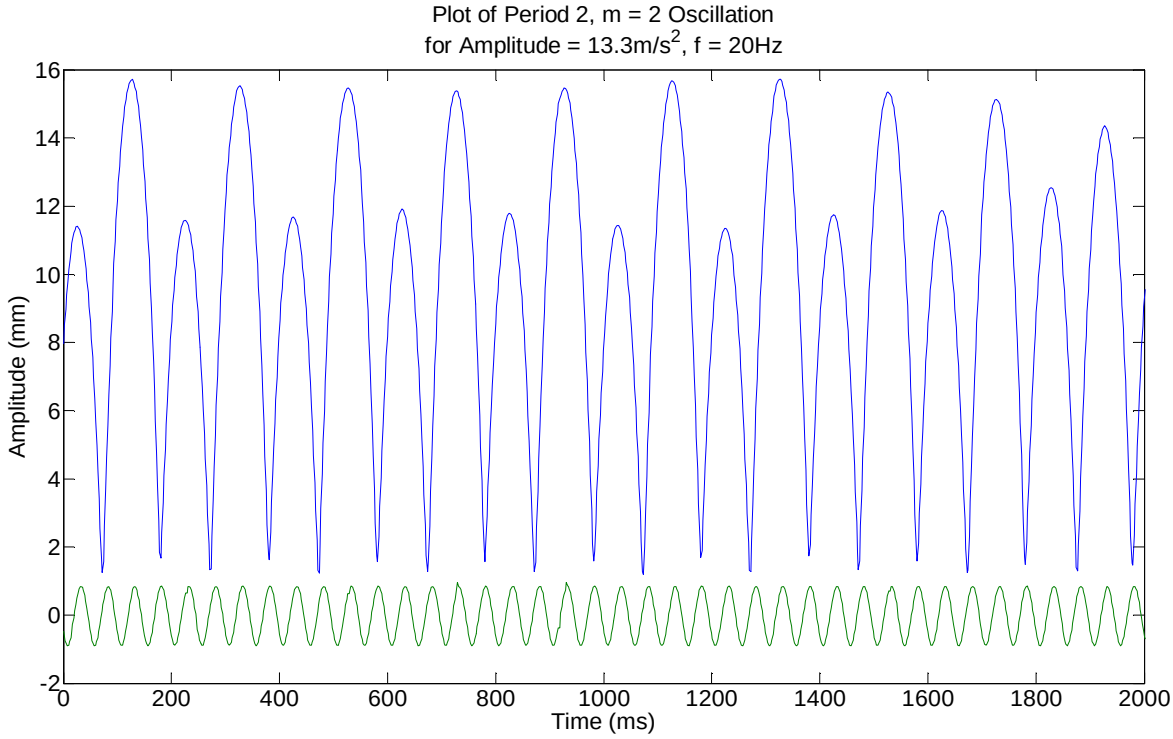

Figure 3.7. Period 2 Behavior with m = 2 as Captured by the Vision System

D. Putting it All Together – Bifurcation Diagrams.

By starting the ball bouncing at relatively low amplitude, and slowly increasing the maximum acceleration of the bar over a long period of time, it is possible to create a bifurcation diagram such as the one in Figure 3.8.

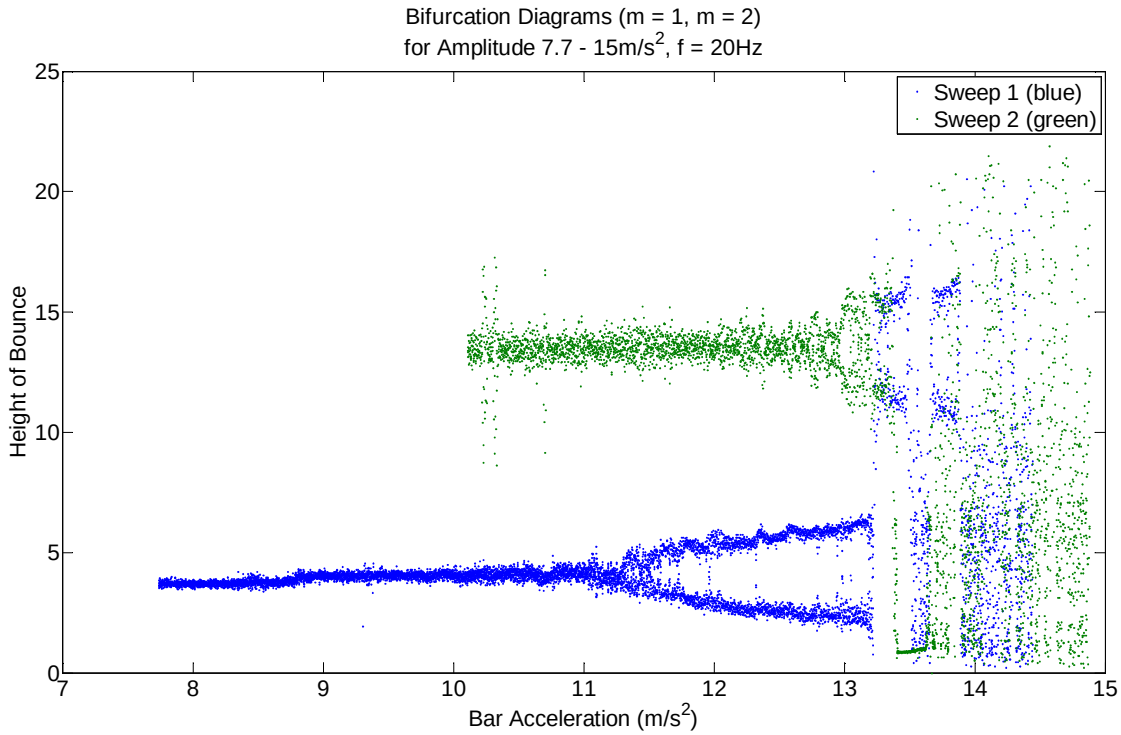

Figure 3.8. Bifurcation Diagram Created from Experimental Data

The data displayed in the plot was captured using the same experimental setup as in the period 3 example. The plot consists of two separate sweeps. Data from the first sweep is shown in blue and the bar's maximum acceleration was governed by the equation:

$$Acc(t) = 0.0128t + 7.74$$

The second sweep was conducted using the same method, but the ball was given a larger initial energy, and the sweep covered a different range of amplitudes. The governing equation for the second sweep, shown in green, is given by:

$$Acc(t) = 0.0123t + 10.12$$

In both cases, the bifurcation diagram was created by calculated the maxima of each ball bounce, using the same parabolic fit method introduced in section 3A.

Not only does this figure demonstrate a very clear bifurcation at around 11.2m/s^2, but it also captures a second bifurcation, shown mostly in green. This illustrates a very important concept, which is the existence of bifurcations at different values of m. The bifurcation for m = 1 is shown in blue, and the bifurcation for m = 2 is shown mostly in green.

The same plot was generated using a simulation written in Matlab. The simulation uses a binary search to calculate the intersection of a point, traveling in a parabolic arch, with a sin curve. The results of the simulation are displayed in Figure 3.9.

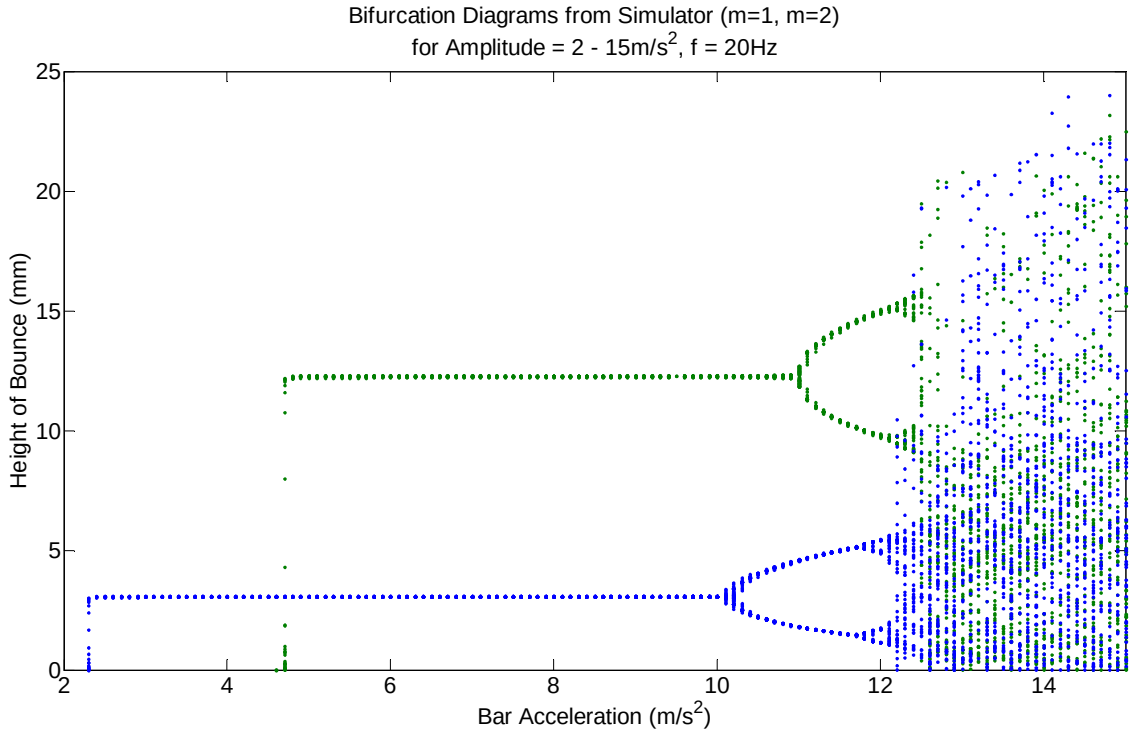

Figure 3.9. Bifurcation Diagram Created from Simulator

As shown in the figure, the simulator yielded very similar results. There are some small differences, however. First of all, while both the simulator and experimental setup produced very similar values for the ball's amplitude, the accelerations at which these amplitudes occur are slightly different. This is most likely due to the assumption of finite restitution. The coefficient of restitution between the ball and the glass lens was experimentally determined by taking several traces of the ball bouncing being dropped on the bar and watching it decay. An average value for the coefficient of restitution was calculated to be 0.856. This value was plugged into the simulator to create the bifurcations above. In practice, however, there was a great variation in the C.o.R. values, and the plastic balls used in the experiments were far from perfect. The simulator also shows the ball continuing to bounce at extremely low amplitudes down to nearly $2 m/s^2$. In practice, this would never be feasible, but theory shows that the stable fixed point still exists at these low amplitudes.

Lowering the coefficient of restitution to 0.75 in the simulator produced results that correlated much more closely to the experimental results. In Figure 3.10, the results from the simulator are plotted on top of the experimental bifurcations from Figure 3.8.

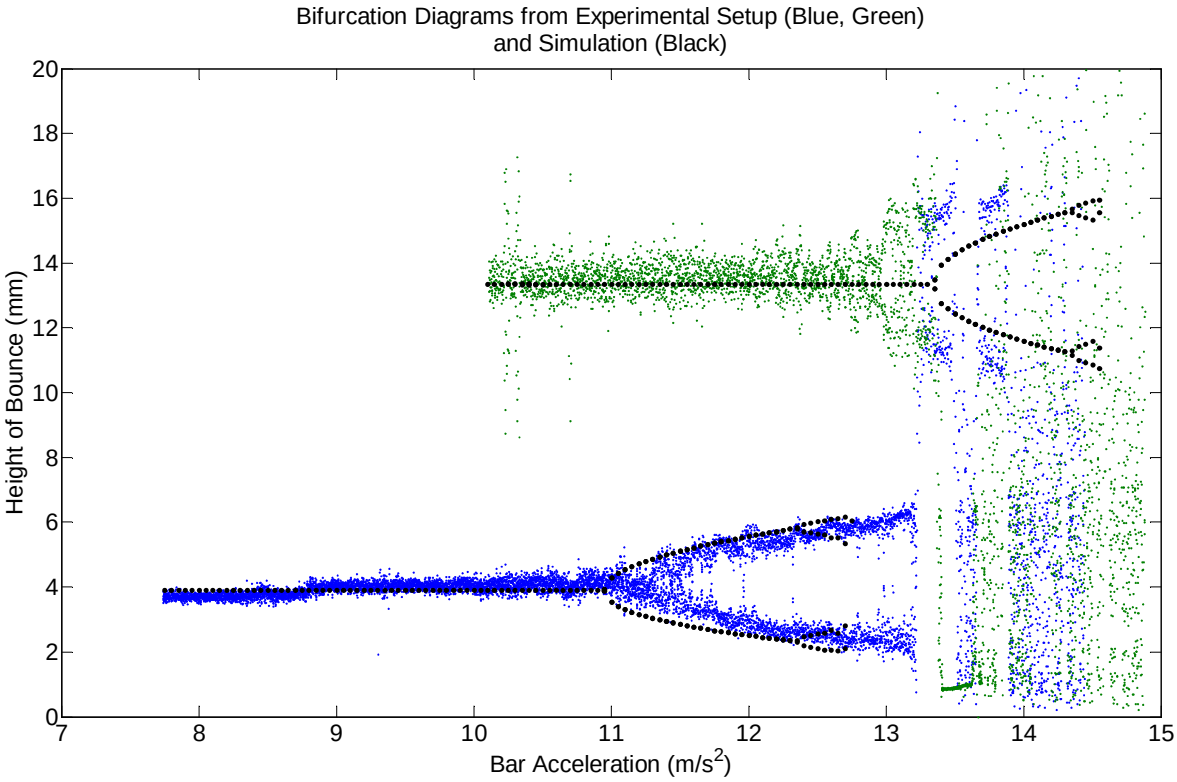

Figure 3.10. Both Experimental and Simulated Bifurcations for m = 1,2

As shown in the figure, for a coefficient of restitution of 0.75, the simulator shows the bifurcation at m=1 occurring slightly earlier than in experiment. For the m = 2 case on the other hand, the bifurcation appears to occur before the predicted value. However, both the height of the bounces and the shape of the bifurcations agree strongly.

If we continue to increase the value of m, so that the ball is bouncing every third or fourth cycle, a pattern begins to emerge as shown in Figure 3.11.

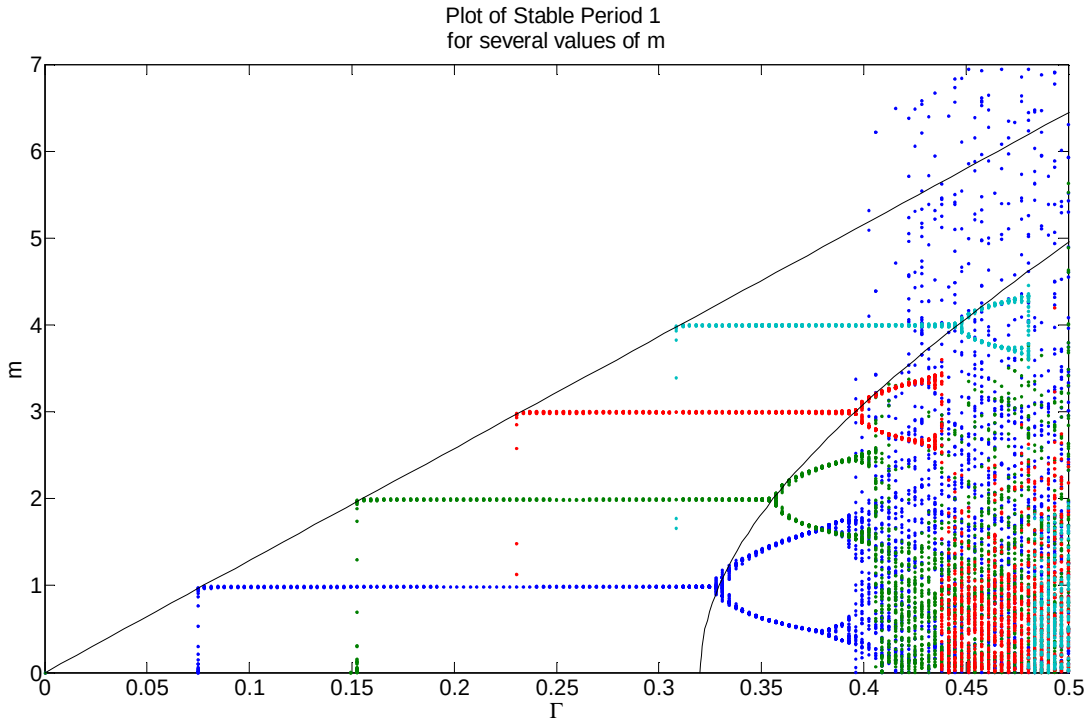

Figure 3.11. Bifurcation Diagrams for Several Values of m

In this figure, gamma is equal to the nondimensionalized acceleration as defined by "Bouncing Ball with Finite Restitution" by Luck and Mehta. It is given by

$$\Gamma = \frac{A\omega^2}{\pi g}$$

Luck and Mehta's paper shows defines the region within which a stable period 1 exists for all values of m. The lower bound of this region is given by

$$\frac{1-\alpha}{1+\alpha} m$$

where alpha is equal to the coefficient of restitution. The upper bound is defined by

$$\left\{ \left[\frac{1-\alpha}{1+\alpha} m \right]^2 + \left[\frac{2(1+\alpha^2)}{\pi(1+\alpha)^2} \right]^2 \right\}^{\frac{1}{2}}$$

where the upper bound is asymptotically approaching the lower bound.

Another way of illustrating the system is displayed in Figure 3.12. This figure uses experimental data to replicate the results found using simulation in the Luck and Mehta paper. It shows reduced phase space of the system. Each point on the scatterplot represents an impact, where tau is equal to the phase of the bar at impact, and W is equal to the relative velocity between the bar and the ball. As shown in the figure, the points cluster around spiraling lines given by the equation

$$W \approx \alpha[\tau + n + \Gamma \cos(2\pi\tau)]$$

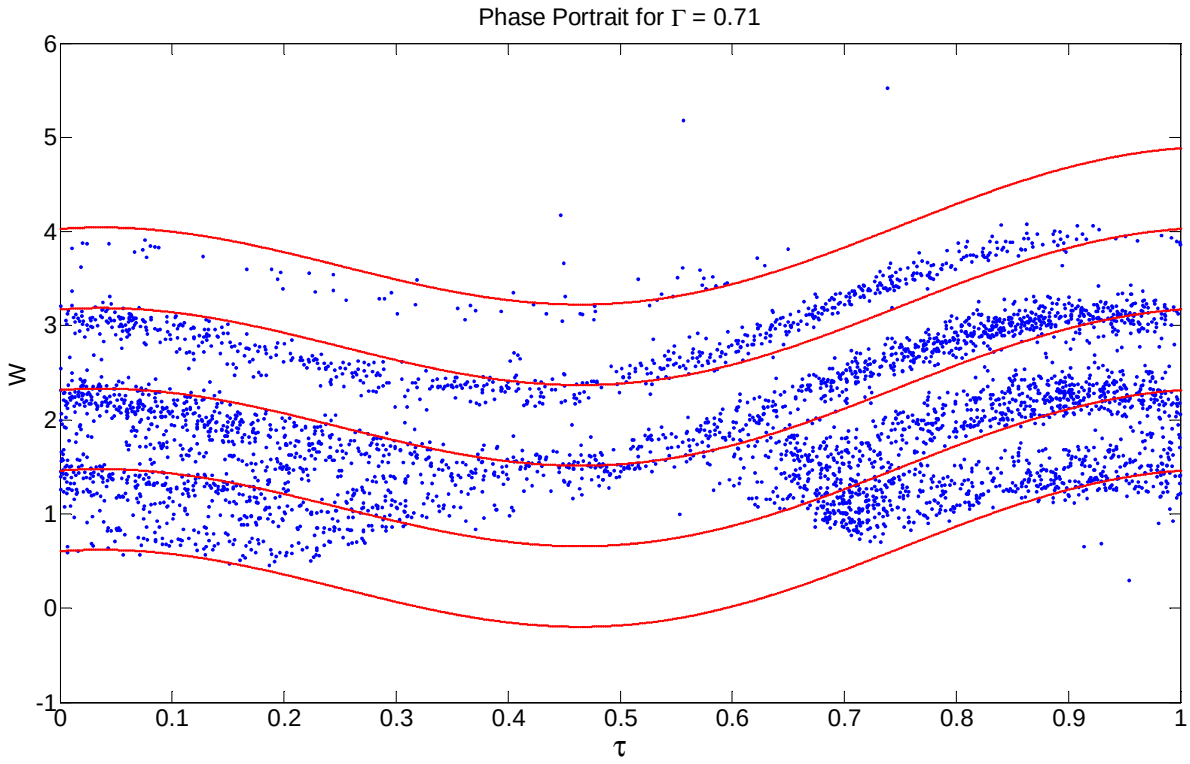

Figure 3.12. Phase Portrait, Generated from Experimental Data

IV. Horizontal Stability.

After investigating vertical stability, the simulator was modified to see if bar motions exist that will stabilize the ball in the x direction. To begin with, a simple motion was investigated which adds motion in the theta direction. A small angular motion was introduced at half the frequency of the vertical motion. The phase between the two motions was then varied to see if one of the phase values would cause side-to-side stabilization. The results of these first simulations are shown in Figure 4.1, where φ_θ is equal to the phase of the angular component relative to the vertical component, and γ describes how fast the ball is sourcing or sinking, as described by the equation $e^{\pm\gamma t}$. All parameters used in the simulator have been nondimensionalized, so the value γ has been normalized by the base frequency.

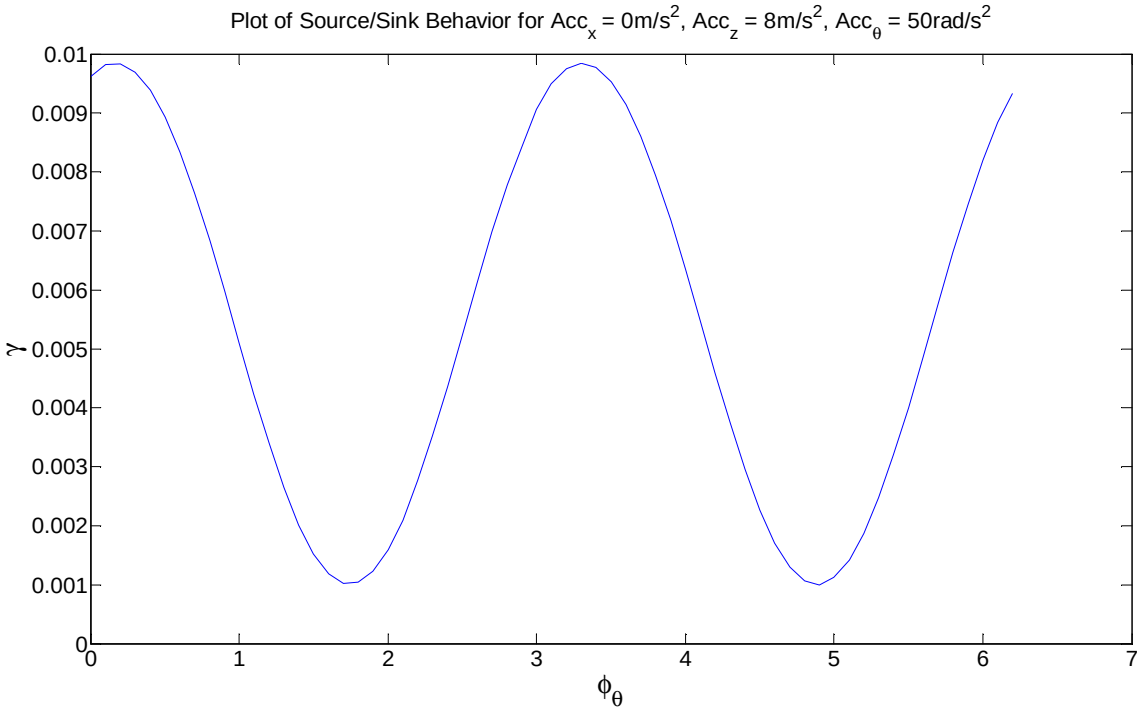

Figure 4.1. Plot of Source/Sink Behavior with Angular Motion, no x-Motion

As indicated by the figure, since gamma never dips below zero, this motion of the bar always causes the ball to exponentially deviate from the center of the bar.

This same motion was used to generate the surface plots in Figures 4.2 and 4.3. These figures illustrate the effect on gamma of varying the theta acceleration and phase.

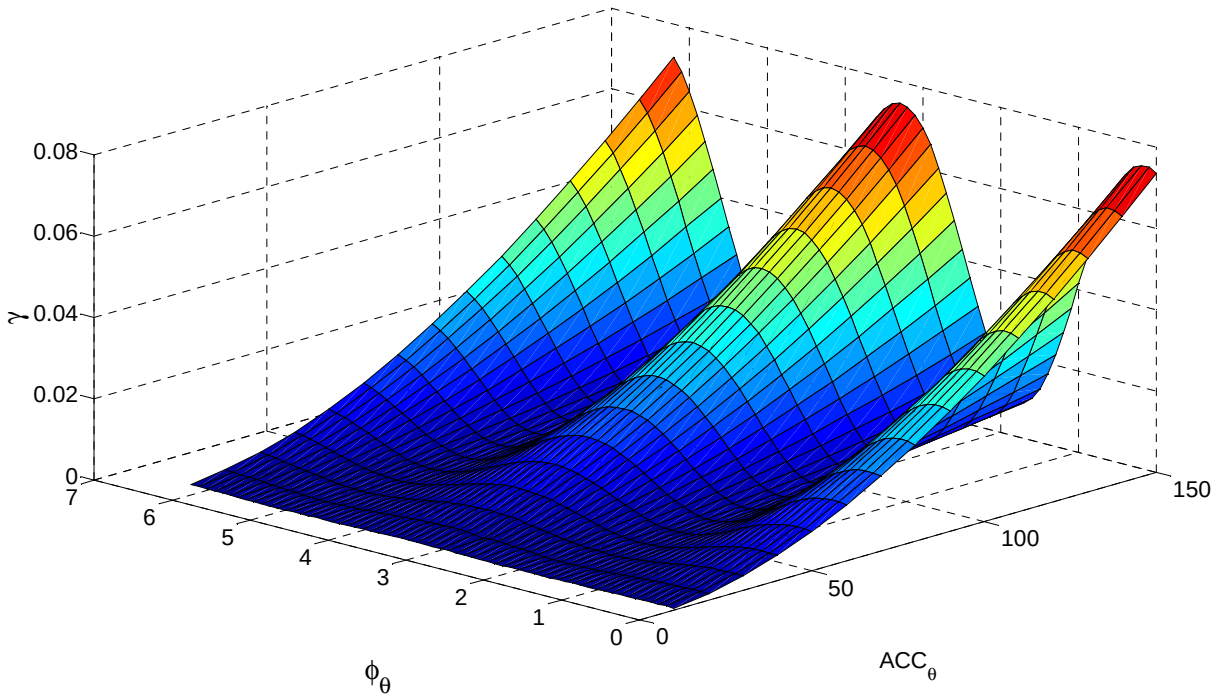

Figure 4.2. Surface Plot of Gamma v. Phase v. Acceleration

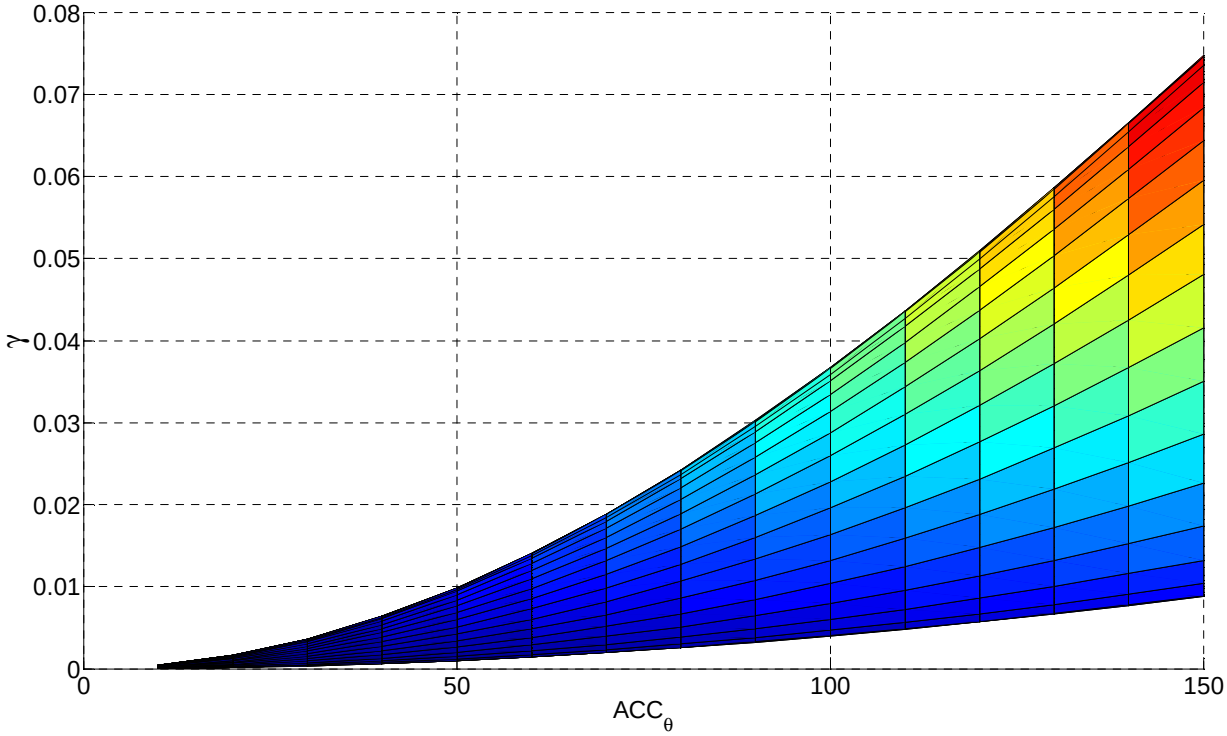

Figure 4.3. Effect of Varying Angular Acceleration on Gamma

Since this simple motion did not stabilize the ball, motion in the x-direction was added in addition to the theta and z motions. By adding motion in the x-direction and varying the phases and frequencies of each component, many different motions become possible. One such motion is shown in Figure 4.4, where the blue traces describe the motion of the bar's centroid.

An in-depth study of the parabolic motion in Figure 4.4 was conducted. The following equations describe the motion used in the following simulations:

$$x(t) = A_x \sin(\omega t + \frac{\pi}{2})$$

$$z(t) = A_z \sin(2\omega t + \frac{\pi}{2})$$

$$\theta(t) = A_\theta \sin(\omega t + \varphi)$$

An illustration of the motion described by these equations is shown below.

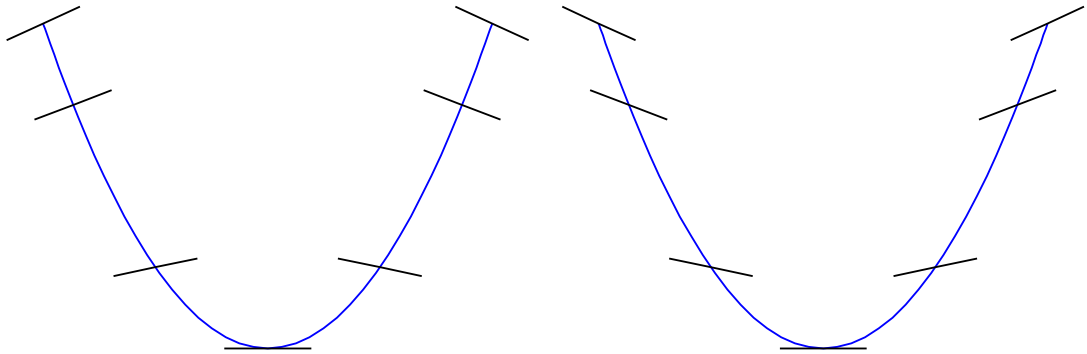

Figure 4.4. Two Possible Bar Motions.

In this case, $\varphi = -\pi/2$ for this first illustration, and $+\pi/2$ for the second illustration. The illustration on the left is actually a motion that will cause source-like behavior, whereas the illustration on the right will cause sink-like behavior.

Introducing a small component in the x-direction to the motion of the bar leads to a modification of the behavior from Figure 4.1. As shown in Figure 4.5, this new x-motion causes the sin wave from Figure 4.1 to be distorted in the center. Some values for gamma are now negative.

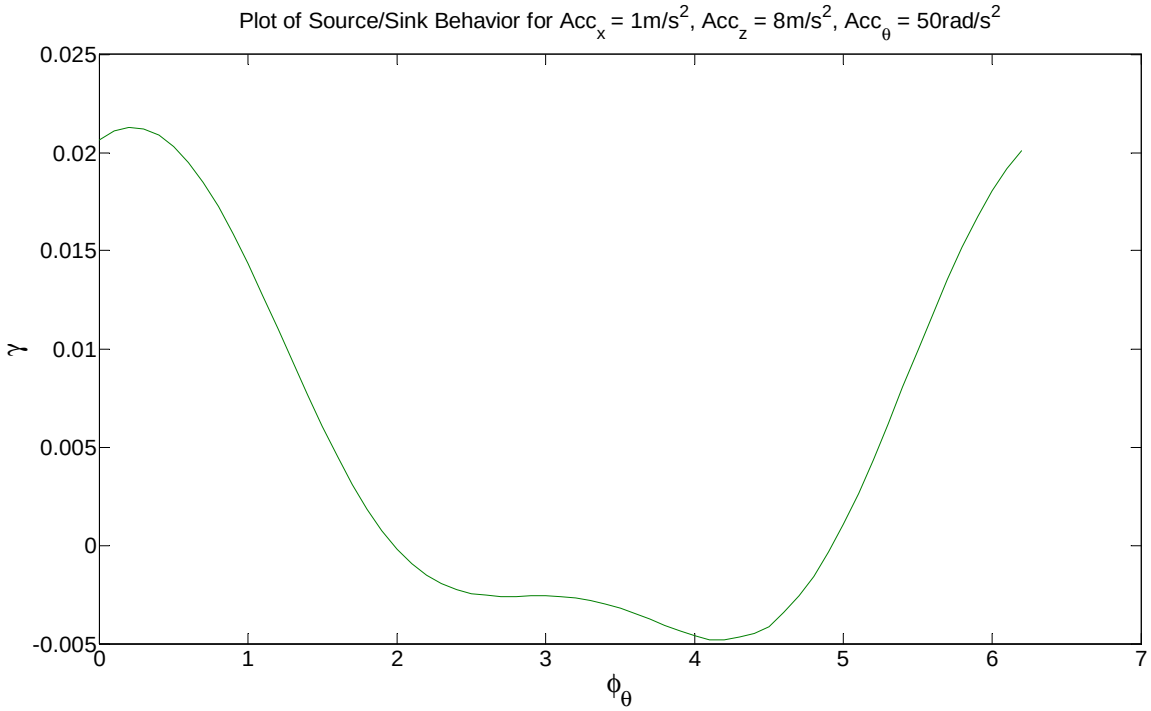

Figure 4.5. Adding a Small Component in the x-Direction

The corresponding surface plot is shown in Figure 4.6.

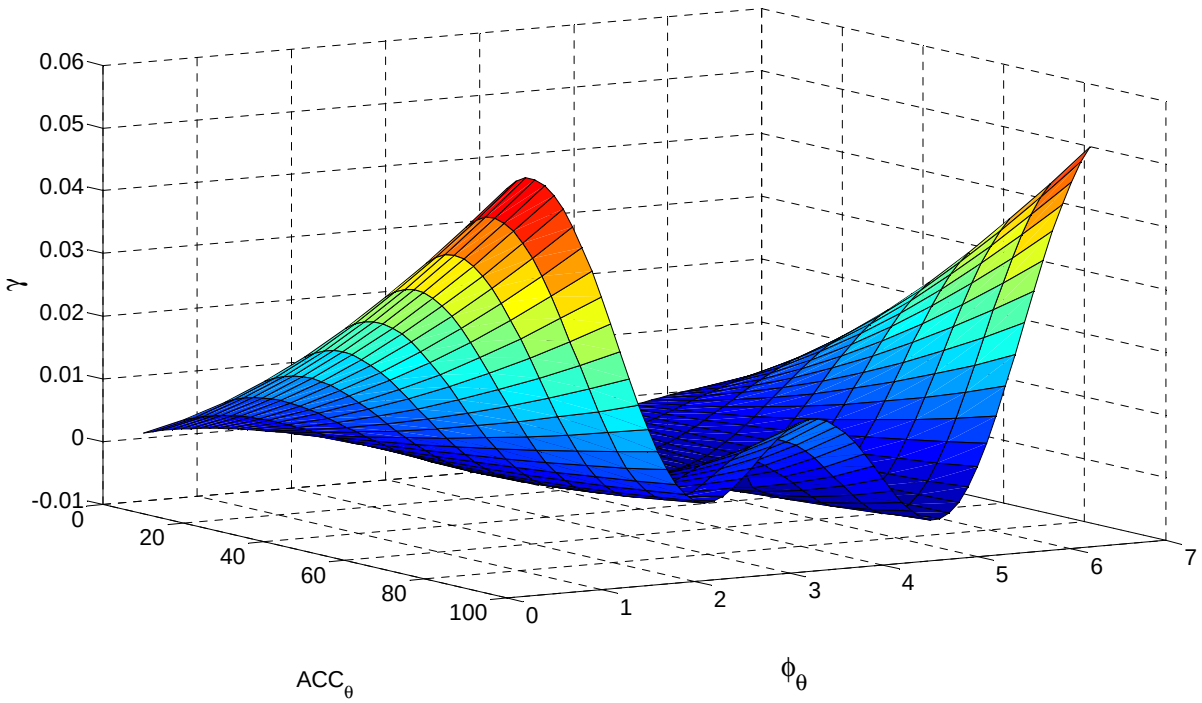

Figure 4.6. Adding a Small Component in the x-Direction

Continuing to increase the amplitude of this motion leads to an even stronger effect as shown in Figure 4.6.

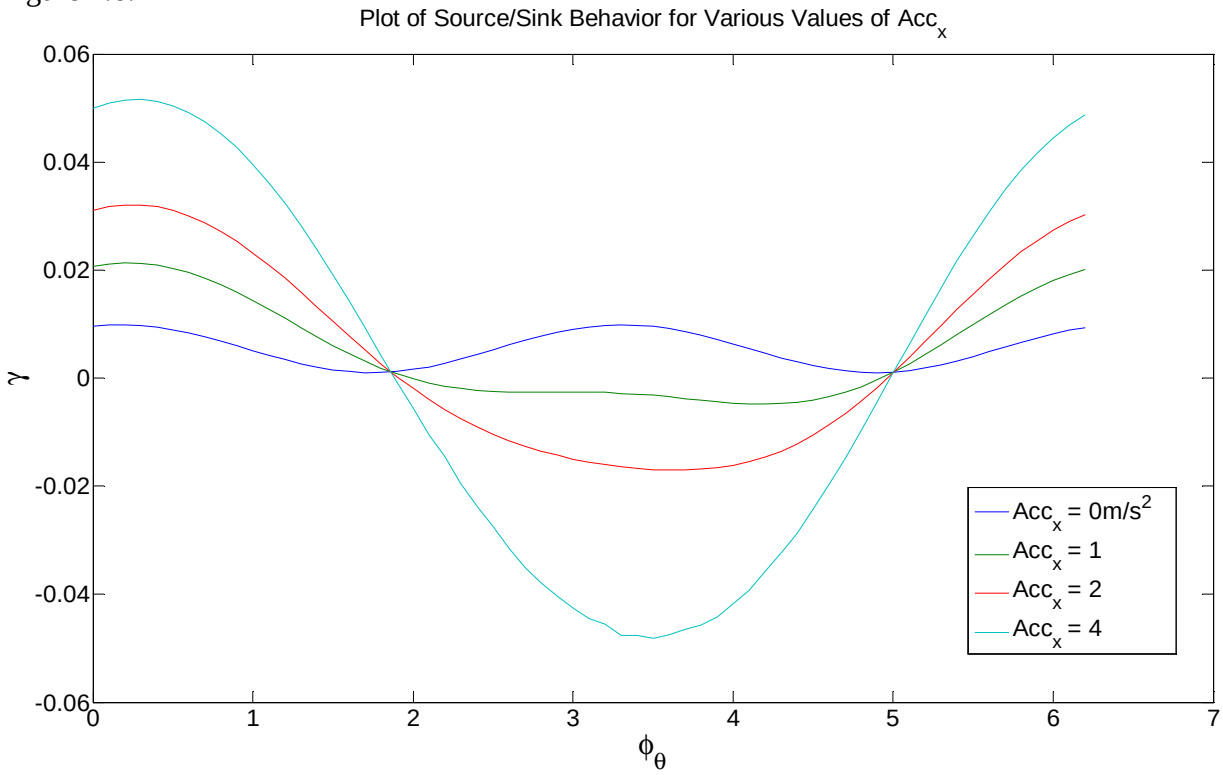

Figure 4.7. Source/Sink Behavior for Several Different Values of x-Amplitude

For a large enough x-amplitude, the repeated sin curve from Figure 1 becomes a single sin curve, which is now more or less centered on the x-axis. For this motion of the bar, the ball will exponentially approach the center of the bar for approximately half the values of phi, and exponentially diverge from the center for the other half.

V. Conclusion.

Ultimately, while some unanswered questions still exist, a great deal was accomplished regarding bifurcation, and vertical and horizontal stability. To begin with, the ability to capture three-dimensional experimental data using the vision system allows experimental verification of theoretical concepts. The vision system was used to capture examples of period 1, period 2 and period 3 behavior as well as period 1 m=2 and period 2 m=2. This data can be used to calculate phases at impact among other things. Furthermore, actual bifurcation diagrams were created by gradually ramping up the acceleration of the bar. Stability in the horizontal direction proved somewhat more difficult. Results from simulation suggest that a simple motion including vertical as well as angular motion will not stabilize the bouncing ball, but rather will always cause it to move away from the center of the bar. Adding an additional motion in the x-direction, however, will sometimes cause source behavior and sometimes cause sink behavior. Increasing the amplitude of the x motion will magnify gamma. Although results from the simulator are promising, experimental verification was never attempted. This would be a significant next step in the study of bouncing ball stability.

References

Anath Kini, Thomas L. Vincent, Brad Paden. “The Bouncing Ball Apparatus as an Experimental Tool.” ASME, Volume 128. June 2006.

H. S. Wright, M. R. Swift, and P. J. King. “The Horizontal Stability of a Ball Bouncing Upon a Vertically Vibrated Concave Surface.” EPL Journal. January, 2008.

J. M. Luck and Anita Mehta. “Bouncing Ball with a Finite Restitution: Chattering, Locking, and Chaos.” Physical Review E, Volume 48, Number 5. November 1993.

N. B. Tufillaro and A.M. Albano. “Chaotic Dynamics of a Bouncing Ball.” Am. J. Phys. 54. October 1986.

Nina B. Zumel and Michael A. Erdman. “Balancing of a Planar Bouncing Object”

Piotr Pieranski and Jerzy Malecki. “Noisy Precursors and Resonant Properties of the Period Doubling Modes in a Nonlinear Dynamical System.” Physical Review A, Volume 31 Number 1. July 1986.

Yu Wang, and Matthew T. Mason. “Two-Dimensional Rigid-Body Collisions with Friction.” Journal of Applied Mechanics, Volume 59. September 1992.